Phase response approaches to neural activity models with distributed delay

Marius Winkler, Grégory Dumont, Eckehard Schöll, Boris Gutkin

Noname manuscript No.
(will be inserted by the editor)

Phase Response Approaches to Neural Activity Models with Distributed Delay

Marius Winkler[1,2] · **Grégory Dumont**[1] · **Eckehard Schöll**[2,4,5] · **Boris Gutkin**[1,3,*]

Received: date / Accepted: date - (The correct dates will be entered by the editor)

Abstract In weakly coupled neural oscillator networks describing brain dynamics the coupling delay is often distributed. We present a theoretical framework to calculate the phase response curve of distributed-delay induced limit cycles with infinite-dimensional phase space. Extending previous works, in which non-delayed or discrete-delay systems were investigated, we develop analytical results for phase response curves of oscillatory systems with distributed delay using Gaussian and log-normal delay distributions.

We determine the scalar product and normalization condition for the linearized adjoint of the system required for the calculation of the phase response curve. As a paradigmatic example, we apply our technique to the Wilson-Cowan oscillator model of excitatory and inhibitory neuronal populations under the two delay distributions. We calculate and compare the phase response curves for the Gaussian and log-normal delay distributions. The phase response curves obtained from our adjoint calculations match those compiled by the direct perturbation method, thereby proving that the theory of weakly coupled oscillators can be applied successfully for distributed-delay induced limit cycles. We further use the obtained phase response curves to derive phase interaction functions and determine the possible phase locked states of multiple inter-coupled populations to illuminate different synchronization scenarios. In numerical simulations we show that the coupling delay distribution can impact the stability of the synchronization between inter-coupled gamma-oscillatory networks.

Keywords coupled oscillators · distributed delay · phase response curve · Wilson-Cowan model

[1] Group for Neural Theory, LNC INSERM U960, DEC, Ecole Normale Supérieure PSL* University, 24 rue Lhomond, 75005 Paris, France

[2] Institut für Theoretische Physik, Technische Universität Berlin, Hardenbergstrasse 36, 10623 Berlin, Germany

[3] Center for Cognition and Decision Making, Institue for Cognitive Neuroscience, NRU Higher School of Economics, Krivokolenniy sidewalk 3, 101000 Moscow, Russia

[4] Bernstein Center for Computational Neuroscience Berlin, Humboldt-Universität, Philippstraße 13, 10115 Berlin, Germany

[5] Potsdam Institute for Climate Impact Research, Telegrafenberg A 31, 14473 Potsdam, Germany

[*]E-mail: boris.gutkin@ens.fr

1 Introduction

Brain rhythms described by oscillating dynamical systems are ubiquitous phenomena which form a basis for multiple cognitive functions [1]. Coherent oscillations in the brain have been reported across many species to be associated with a variety of cognitive tasks [2]. Our understanding and therapies of various brain pathologies and deficiencies, such as Parkinson's disease and epilepsy, rely heavily on the analysis of synchronization of oscillating neuronal signals [3]. There are numerous types of rhythms in the brain ranging from very slow oscillations with periods of tens of seconds to very fast oscillations with frequencies exceeding 1000 Hz [4]. Gamma oscillations, within the frequency band of $30-150$ Hz, are an intensively studied rhythmic brain activity pattern [5]. Data suggest that the gamma cycle results from emergent dynamics of cortical networks, as a natural consequence of the interplay between interconnected pyramidal cells and subnetworks of interneurons [6, 7].

Although these gamma rhythms emerge locally [7], they can interact coherently across the cerebral cortex [8, 9] and show multiple phase relationships that are persistent across time [10].

We note that the brain functional connectome can be modulated by macroscopic rhythms, without the need to alter underlying structural anatomical connectivity [10]. In fact, the functional connectivity depends on the relative phase relationships between the communicating sub-networks. The relative phase relationship does not have to be zero, but depends on the properties of the working neuronal groups and the distance between them [11, 12].

Hence, by understanding and controlling the oscillatory dynamics one can control dynamically the flow of information without changing the structural connectivity. In the past years, the role of gamma patterns and gamma interactions have attracted much attention. However, the issue how to characterize functional connectivities associated with various phase locked states when complex coupling delays are present remains an open question.

Here, we approach this question by studying synchronization of oscillations under synaptic and conduction delays in neural circuits, where such delays may be distributed as opposed to a single discrete delay.

When an oscillator is perturbed by a transient external stimulus, the trajectory is displaced from its limit cycle, potentially resulting in a phase shift of the oscillation. Phase shifts due to the perturbations of the oscillator, that come at different phases within the limit cycle, are described by the so-called phase response curves (PRC) [13–19]. Phase response curves can be computed directly for any rhythm by applying short pulses at different phases of the cycle and measuring the phase shift. They can be used to study weakly perturbed nonlinear oscillators and predict synchronization properties in neuronal networks [20–22]. They can be measured for random disturbances both experimentally and numerically. It is important that enough time elapses after a disturbance, that the perturbations are infinitesimally small and that the disturbed trajectory can relax back to the limit cycle. For perturbations that are infinitesimally small in duration and in amplitude, one obtains the infinitesimal phase response curve (iPRC) [23]. The adjoint method allows one to reduce the dynamics of each neuron, which may be of very high dimension, to a single differential equation – the adjoint equation – describing the phase of the neuron [24].

When analyzing neural dynamics, it is important to take into account that time delays in the interconnections can substantially influence emergent dynamics. These delays arise naturally in many neuronal but also optical, electronic, or technological systems due to finite signal transmission and processing times [25–30]. Delays can be assumed to be either discrete or distributed. In general, we may assume that connectivity delays, stemming from synaptic as well as axonal conduction delays, have a bell-shaped distribution such as Gaussian instead of being discrete. However, at physiological and anatomical levels in the brain many parameters, such as synaptic weights, the firing rates of individual neurons, or the discharge of neuronal populations, has been shown to have skewed distributions with a heavy tail [31]. Therefore, it is reasonable to consider a log-normal distribution as well, in addition to a Gaussian distribution. In this paper we go beyond previous works, in which undelayed or discrete-delay systems were investigated [17], by developing analytical results for phase response curves of distributed delay systems for Gaussian and log-normal delay distributions.

According to the recently advanced Communication through Coherence hypothesis, neuronal interaction and information transmission is dynamically shaped by the phase relationship between the neural oscillations [8, 32]. These relationships have been shown to be diverse and can arise due to a diversity of connection delays [33]. Applying the adjoint theory to brain dynamics is a useful tool, since it allows for reduction of the dynamics to a single equation for the phase. Thus, weakly perturbed oscillators can be studied more efficiently for the corresponding control parameters, and synchronization properties in neural networks can be investigated on a broad spectrum of different settings.

We apply our methodology to the pyramidal-interneuronal network gamma (PING) rhythm [33]. The underlying dynamics for the considered PING model are the Wilson-Cowan equations which include one equation for the excitatory cells and one equation for the inhibitory cells. The Wilson-Cowan dynamics describe the time evolution of the activity of populations of neurons, using a nonlinear sigmoidal function to represent the interactions between the populations, resulting in a stable limit cycle solution. The Wilson-Cowan model has been the starting point for many extensions; it represents one of paradigmatic models in theoretical neuroscience.

In this work we use the Wilson-Cowan (PING) model, and introduce a theoretical framework to calculate the phase response function. To this purpose, we determine the scalar product required in the mathematical formalism and the normalization condition for the linearized adjoint equations of the system. We show that the adjoint theory can be extended to distributed delays by matching the phase response curves obtained by the direct and adjoint methods. We apply our theory to discrete, Gaussian, and log-normal delay distributions and use the interaction function that determines the possible phase locked states to illuminate different synchronization scenarios. In Sect. 2 we introduce the method including the Wilson-Cowan model, the distributed delay, the adjoint theory, and the interaction function. In Sect. 3 we present the results, which are discussed in Sect. 4. Finally, in Sect. 5 we conclude.

2 Method

2.1 Wilson-Cowan Dynamics

The Wilson-Cowan model [34], also known as the Pyramidal Interneuron Network Gamma (PING) model, describes the behaviour of a synaptically coupled neuronal network of excitatory and inhibitory neurons. The model has a stable limit cycle solution, which we consider in the following. The system is not a detailed biophysical model, but a coarse-grained description of the overall activity of a large-scale neuronal network, based upon two differential equations for the populations of excitatory and inhibitory neurons, E(t) and I(t), respectively [35]:

$$\begin{aligned}\frac{\mathrm{d}}{\mathrm{dt}}\mathrm{E}(t) &= -\mathrm{E}(t)+w_{ee}\cdot f\big[\mathrm{E}(t)\big]-w_{ei}\cdot f\big[\mathrm{I}(t)\big]+i_e\\ \frac{\mathrm{d}}{\mathrm{dt}}\,\mathrm{I}(t) &= -\mathrm{I}(t)+w_{ie}\cdot f\big[\mathrm{E}(t)\big]-w_{ii}\cdot f\big[\mathrm{I}(t)\big]+i_i\end{aligned} \tag{1}$$

with the non-linear sigmoid function modelling the synaptic input:

$$f(s)=\frac{1}{1+e^{-s}}$$

Important parameters in the model are the coefficients w_{ee}, w_{ii}, w_{ei}, w_{ie} which are called synaptic weights and denote the strength of connectivity within the excitatory and inhibitory, and between the excitatory and inhibitory populations, respectively. The parameters i_e and i_i denote the external inputs to the excitatory and inhibitory neurons. The variables E and I are associated with the mean action potential (voltage) of the excitatory and inhibitory neuronal populations, respectively. After a transient the system reaches a limit cycle oscillation.

2.2 Distributed Delay

Delayed processes are ubiquitous in physical, chemical and especially biological systems [36–40]. Typically time delays reflect a combination of transmission and processing times or the time it takes to react to a stimulus. Examples of transmission times are the propagation time and the conduction time along an axon which can range from the order of 1 ms along unmyelinated axons for example in the grey matter to more than 100 ms along myelinated axons [41]. Examples of processing time are the time it takes to synthesize red blood cells in the bone marrow ($\approx 5-7$ days) [42], or the time it takes animals to mature to reproductive age (weeks to months) [39], or the time it takes a chemical synapse to process an incoming action potential in the presynaptic terminal to a potential change in the postsynaptic cell. Systems with time delays are often characterized by delay differential equations (DDEs). Time delay can substantially influence emergent dynamics. For instance, delays can either induce instabilities and bifurcations of dynamical systems or stabilize unstable states such as in chaos control by time delayed feedback [43], and suppress or enhance synchronization [44]. Delay may be introduced artificially by external feedback loops, and it may also arise naturally in many neuronal, optical, electronic, or technological systems due to finite signal transmission and processing times.

In typical processes in nature, for example in complex networks [44–48] and in particular in biological systems [49–51], it is reasonable to assume that the delay times are not fixed at a single value τ but are distributed. For example, along unmyelinated axons in the grey matter the diameters of the axons obey a distribution, which implies that the axonal conduction velocities are also distributed. Then the delay can be expressed as a convolution integral with a delay kernel:

$$\mathrm{X}(\mathrm{t}-\tau)\to\int_0^{+\infty}\mathrm{ds}\;\;\Delta_\mathrm{i}(s)\mathrm{X}(\mathrm{t}-\mathrm{s}), \tag{2}$$

where $\Delta_\mathrm{i}(s)$ is an integral kernel that describes the distribution of delays.

In many cases a **Gaussian distribution** gives a good approximation for the normalized delay kernel

$$\Delta_\mathrm{G}(s)=\frac{1}{\sqrt{2\pi}\cdot\sigma}e^{-\frac{(s-\tau)^2}{2\sigma^2}}, \tag{3}$$

with the standard deviation σ and mean delay time τ. In the neural context, however, often the distributions of various parameters are asymmetric with a heavy tail [31]. Then the **log-normal distribution** provides more realistic results for the simulation of biological processes:

$$\Delta_\mathrm{L}(s)=\frac{1}{\sqrt{2\pi}\cdot\sigma s}e^{-\frac{(\ln(s)-\tau)^2}{2\sigma^2}}, \tag{4}$$

with the standard deviation σ and mean delay time τ.

Fig. 1 shows schematically different types of delay kernels for a sinusoidal solution $X(t)$ of a delay differential equation (black curve). The value $X(t-\tau)$ is convolved (weighted) with the Gaussian delay kernel (purple curve) or with the asymmetric log-normal delay kernel (green).

Fig. 1 shows schematically a sinusoidal solution of a delay differential equation (black curve) which depends on the past in a way that the discrete value, with difference τ at time t is chosen as mean μ, and all function values left and right of the mean are weighted Gaussian-like (purple/dark-grey curve) with the standard deviation σ.

In conclusion, we obtain the following system of equations for the Wilson-Cowan model with distributed delay in the coupling:

$$\begin{aligned}\frac{\mathrm{d}}{\mathrm{dt}}\mathrm{E}(t) &= -\mathrm{E}(t)+w_{ee}f\left[\Delta_i^E(t)\right]-w_{ei}f\left[\Delta_i^I(t)\right]+i_e\\ \frac{\mathrm{d}}{\mathrm{dt}}\,\mathrm{I}(t) &= -\mathrm{I}(t)\;+w_{ie}f\left[\Delta_i^E(t)\right]-w_{ii}f\left[\Delta_i^I(t)\right]+i_i,\end{aligned} \tag{5}$$

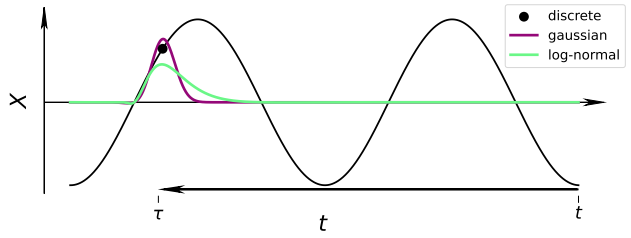

Fig. 1 Schematic representation of distributed delay kernels. The sinusoidal solution $X(t)$ of a delay differential equation (black curve) is shown. The distributed delay is given by $X(t-\tau)$ (black dot) weighted with the Gaussian (purple curve) or the log-normal (green curve) delay kernel in a convolution integral. Both integral kernels are normalized to 1.

where $\Delta_i^E(t)$ and $\Delta_i^I(t)$ are the distributed delay kernels, see Eq. (2), for the excitatory

$$\Delta_i^E(t) = \int_0^{+\infty} \mathrm{ds}\ \ \Delta_\mathrm{i}(s)\mathrm{E}(\mathrm{t}-\mathrm{s})$$

and for the inhibitory population

$$\Delta_i^I(t) = \int_0^{+\infty} \mathrm{ds}\ \ \Delta_\mathrm{i}(s)\mathrm{I}(\mathrm{t}-\mathrm{s}),$$

respectively, and the subscripts $i = G$ (Eq. 3) and $i = L$ (Eq. 4) denote the Gaussian or log-normal distributions, respectively.

2.3 Applying the Adjoint Theory

In this study, we develop an adjoint method [24] to compute the phase response curve $\mathrm{Z}(\theta)$ for limit cycles exhibited by DDEs. A key ingredient is the introduction of a mathematically appropriate scalar product for differential equations with distributed delay, which enables us to properly define the phase θ and calculate $\mathrm{Z}(\theta)$ for limit cycles in infinite-dimensional phase space.
The first task is to derive a phase response curve $\mathrm{Z}(\theta)$ for perturbations of a DDE with fixed delay τ of the form

$$\frac{\mathrm{d}}{\mathrm{dt}}\mathrm{X(t)} = \mathrm{F}\big(\mathrm{X(t)}, \mathrm{X(t-\tau)}\big), \tag{6}$$

where $\mathrm{X(t)} \in \mathbb{R}^N$ is a column vector of N real components and τ is a nonnegative constant delay. We assume that this DDE has a stable limit cycle solution $\mathrm{X}_0(\mathrm{t})$. If a small perturbation ε is applied to the limit cycle, the perturbed solution can be written as $\mathrm{X(t)} = X_0(t) + \varepsilon \mathrm{X_p(t)}$ with the perturbed part $\mathrm{X_p(t)}$. From linearization around the unperturbed solution it follows that the perturbation obeys

$$\frac{\mathrm{d}}{\mathrm{dt}}\mathrm{X_p(t)} = \mathrm{DF_1(t)X_p(t)} + \mathrm{DF_2(t)X_p(t-\tau)}, \tag{7}$$

where $\mathrm{DF_1}$ and $\mathrm{DF_2}$ refer to the Jacobian matrices of F with respect to $\mathrm{X(t)}$ and $\mathrm{X(t-\tau)}$, respectively, taken at $\mathrm{X}_0(\mathrm{t})$, $\mathrm{X}_0(\mathrm{t}-\tau)$ [14, 17, 18].

The infinitesimal phase response curve $\mathrm{Z}(\theta)$ quantifies the linear response of the oscillator phase θ to the applied perturbations. It is the solution of [17]:

$$\frac{\mathrm{d}}{\mathrm{dt}}\left\langle \mathrm{Z}(t), \mathrm{X_p}(t) \right\rangle \stackrel{!}{=} 0. \tag{8}$$

where the exclamation mark denotes the imposed condition. Here, we need an appropriate scalar product to derive the adjoint equation for Z(t). For distributed differential delay equations this scalar product is appropriately defined by:

$$\begin{aligned}\langle \Psi(t), \Phi(t) \rangle &= \Psi(t)\Phi(t) \\ &+ \int_0^{+\infty} ds\Delta(s) \int_{t-s}^{t} d\xi \Psi(\xi+s)\mathrm{DF_2}(\xi+s)\Phi(\xi),\end{aligned} \tag{9}$$

where $\mathrm{DF_2(t)}$ is defined in analogy with Eq. 7 as the coefficient of the perturbed linearized equation

$$\frac{\mathrm{d}}{\mathrm{dt}}\mathrm{X_p}(t) = \mathrm{DF_1(t)X_p}(t) + \mathrm{DF_2(t)} \int_0^{+\infty} \mathrm{ds}\ \ \Delta(\mathrm{s})\mathrm{X_p}(t-s).$$

A proof that this is the correct scalar product for distributed differential delay equations is given in the appendix (A).

Applying Eq. (9) to Eq. (8) defines an adjoint equation:

$$-\frac{\mathrm{d}}{\mathrm{dt}}\mathrm{Z(t)} = \mathrm{DF_1(t)^T Z(t)} + \mathrm{DF_2(t+\tau)^T Z(t+\tau)}, \tag{10}$$

where superscript T denotes the transposed matrix. Using the limit cycle solution solution $\mathrm{X}_0(\mathrm{t})$ obtained numerically, we generate the solution $\mathrm{Z(t)}$ of Eq. (10) by integrating backwards in time from arbitrary initial conditions. The limit cycle is asymptotically stable, hence the backwards integration damps out all components except the periodic one which is the solution of the adjoint equation [15].

We further normalize the amplitude of $\mathrm{Z(t)}$ by setting

$$\frac{\mathrm{d}}{\mathrm{dt}}\left\langle \mathrm{Z}(t), \frac{\mathrm{d}}{\mathrm{dt}}\mathrm{X}_0(t) \right\rangle \stackrel{!}{=} 0. \tag{11}$$

This gives us the possibility to compare our results obtained via the adjoint method with results derived by the direct perturbation method. To calculate directly the phase response curve, we apply a weak perturbation to all components of the vector at a chosen phase of the oscillatory cycle, measure the phase shift with respect to the non-perturbed system and track the results for one period of oscillation. A weak perturbation pulse must be considered in order to obtain accurate results. Too strong perturbations will lead the dynamics far away from the limit cycle. In this work we choose a rectangular pulse with variable height and width.

Applying our newly derived adjoint method allows us to calculate the phase response curve $\mathrm{Z}(\theta)$ for a distributed-delay induced limit cycle, given by a delay differential equation with distributed delay kernel of standard deviation σ. This is the main result of this study. If we take the limit $\sigma \to 0$ our method reduces to the discrete delay model and if we further take the limit $\mathrm{DF_2} \to 0$ or $\tau \to 0$ the conventional adjoint method for ordinary differential equations is retrieved.

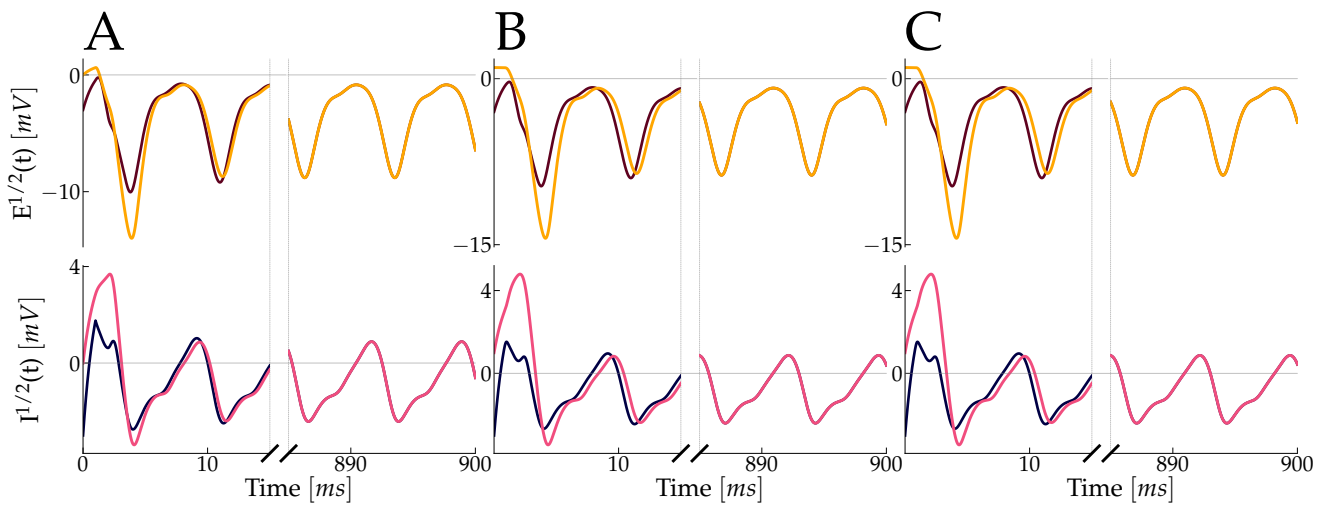

Fig. 2 Phase-locking of two weakly coupled Wilson-Cowan oscillators with A discrete, B Gaussian and C log-normal distributed delay. The upper row in each panel shows the time trace of the two excitatory populations E^1, E^2 and the lower row shows the two inhibitory populations I^1, I^2 for **A** discrete, **B** Gaussian and **C** log-normal distributed delay. In each case the x-axis shows the beginning (no match) and the end of the simulation (phase locking) where the part in between is skipped. Parameters: $w_{ee} = 20, w_{ei} = 21, w_{ie} = 16, w_{ii} = 6, i_e = 1.5, i_i = -0.5, \tau = 1, \sigma = 0.1, C = 0.01$.

2.4 Phase Interaction Function $\mathrm{H}(\phi)$

While the phase response curve is a measure of the phase shift after an infinitesimally small perturbation of the limit cycle for one Wilson-Cowan oscillator, the phase interaction function $\mathrm{H_i}(\phi)$ describes the influence of the interaction of two weakly coupled identical Wilson-Cowan oscillators with phases θ_1 and θ_2 in terms of the difference of their phases $\phi = \theta_2 - \theta_1$ upon their phase dynamics. The interaction function which depends only on the phase difference is computed by the convolution of the phase response function $\mathrm{Z_i(t)}$ with the unperturbed system dynamics $\mathrm{X_{0,i}(t)}$ of oscillator $i = 1, 2$:

$$\mathrm{H_i}(\phi) = \frac{\mathrm{C}}{\mathrm{T}} \int_0^{\mathrm{T}} \mathrm{dt}\ \mathrm{Z_i(t) X_{0,i}(t-\phi)}, \tag{12}$$

with the coupling strength C and the period of the oscillation T . In the special case of symmetric coupling the interaction function is identical for both oscillators $i = 1, 2$, hence $\mathrm{H_1} = \mathrm{H_2} \equiv H$. Therefore, we can set up an equation for the phase-difference:

$$\frac{\mathrm{d}\phi}{\mathrm{dt}} = (\mathrm{H}(\phi) - \mathrm{H}(-\phi)) \equiv \mathrm{G}(\phi) \tag{13}$$

Then, $\mathrm{G}(\phi)$ is the odd part of the interaction function $\mathrm{H}(\phi)$. It is periodic, and its zeros describe phase-locked states ϕ^*; those for which $\mathrm{G}(\phi^*)$ has a positive slope are stable, and those for which $\mathrm{G}(\phi^*)$ has a negative slope are unstable.

The advantage of this reduced description of two coupled oscillators is that it allows one to explore the parameter space in terms of simple phase oscillators. For instance, it has been applied to a ring of N nonlocally coupled FitzHugh-Nagumo oscillators [52] to pinpoint a region in the parameter space which favors the appearance of chimera states.

3 Results

3.1 Unperturbed System Dynamics

The calculation of the phase interaction function $\mathrm{H_i}(\phi)$, as derived in the previous section, requires the unperturbed system dynamics $\mathrm{X_{0,i}(t)}$ and the phase response function $\mathrm{Z_i(t)}$, i.e., these must be computed first for each Wilson-Cowan oscillator, before the convolution integral can be calculated for the pairs of identical Wilson-Cowan oscillators. In order to ensure that the considered system of weakly coupled oscillators is indeed synchronized, we have simulated the coupled system for an appropriate set of parameters numerically for a long time to verify the synchronization.

Fig. 2 shows three panels of time series for **A** discrete, **B** Gaussian distributed and **C** log-normal distributed delay for two coupled Wilson-Cowan oscillators. The upper row in each panel shows the two weakly coupled excitatory populations and the lower row shows the two weakly coupled inhibitory populations. In each case the x-axis shows the beginning (no synchronization) and the end of the simulation (phase synchronization) where the part in between is skipped.

3.2 Phase Response Curves

Fig. 3 shows three panels for a single Wilson-Cowan oscillator with **A** discrete, **B** Gaussian and **C** log-normal distributed delay. In each panel the top left shows the time series of excitatory $\mathrm{E}(t)$ (red) and inhibitory $\mathrm{I}(t)$ (blue) populations. The top right shows the dynamics in phase space $\mathrm{E}(t)$ vs $\mathrm{I}(t)$. The phase response curves in the bottom of

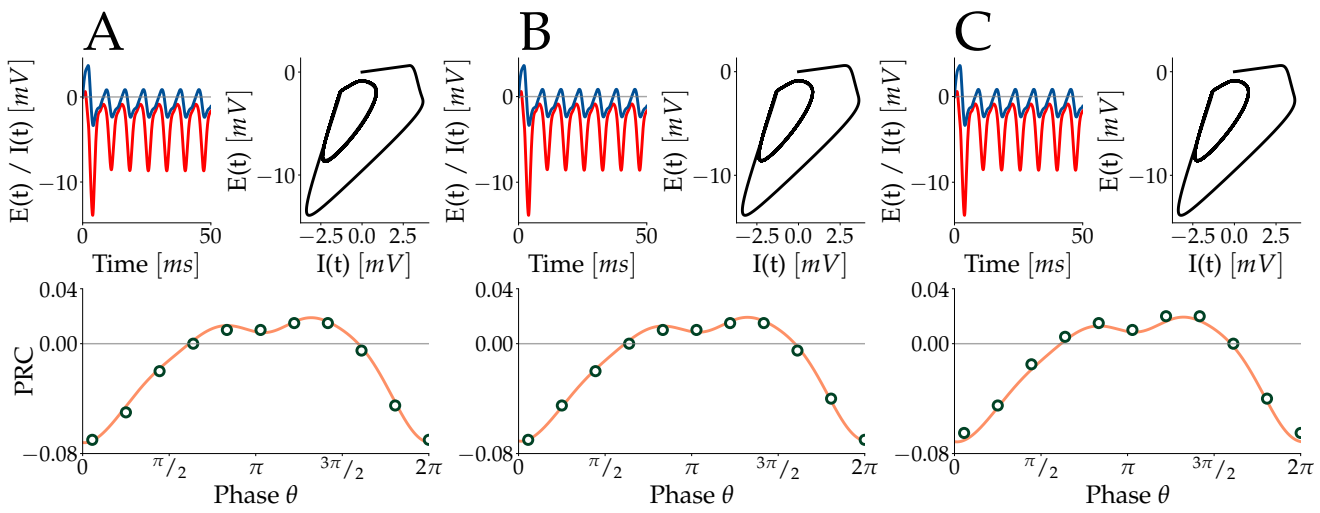

Fig. 3 System dynamics, phase space and phase response curves. The three panels show the solutions of a single Wilson-Cowan model for **A** discrete, **B** Gaussian and **C** log-normal distributed delay. In each panel the top left shows the time traces of the excitatory $E(t)$ (red) and inhibitory $I(t)$ (blue) populations. The top right shows the dynamics in phase space $E(t)$ vs. $I(t)$. The bottom of each panel shows the phase response curves obtained by the direct simulation (green circles) and the adjoint method (orange line; normalized). Parameters: $\tau = -1$, $\sigma = 0.1$, perturbation impulse height $= 0.07$, impulse width $= 1$, $w_{ee} = 20$, $w_{ei} = 21$, $w_{ie} = 16$, $w_{ii} = 6$, $i_e = 1.5$, $i_i = -0.5$.

each panel show that the extension from discrete to Gaussian or log-normal distributed delay does not lead to significant changes in the behavior of the system dynamics. Oscillation period and amplitude remain similar. The small standard deviation of the delay distribution $\sigma = 0.1$ which results in a very sharp Gaussian- or log-normal peak resembles a single discrete value.

The bottom plot of each panel shows a comparison between the phase response curves obtained by direct simulation of a perturbation (green circles) and by the adjoint theory (orange line). The good agreement between the two phase response curves proves that the adjoint theory is not only applicable for non-delayed or discrete delay systems but also for distributed-delay systems with **B** Gaussian and **C** log-normal distributions.

3.3 Distributed Delay effects Phase-Locking

To study the phase dynamics and the effects of the delay distribution characteristics on phase-locked states and synchrony we calculate the function $\mathrm{G}(\phi)$(Eq. 13) for excitatory-excitatory and inhibitory-inhibitory coupled pairs of identical Wilson-Cowan oscillators from the phase interaction function $\mathrm{H}(\phi)$ as introduced in section (2.4) for the Wilson-Cowan model. Fig. 4 shows the interaction functions

$$\mathrm{H_E}(\phi) = \frac{\mathrm{C}}{\mathrm{T}} \int_0^{\mathrm{T}} \mathrm{dt}\ \ \mathrm{Z_E(t) X_{0,E}(t-\phi)}$$

and

$$\mathrm{H_I}(\phi) = \frac{\mathrm{C}}{\mathrm{T}} \int_0^{\mathrm{T}} \mathrm{dt}\ \ \mathrm{Z_I(t) X_{0,I}(t-\phi)}$$

for a pair of identical Wilson-Cowan oscillators. Since the interaction functions for a pair of oscillators are identical under the given conditions, we show the solution for one oscillator only. **A** displays the interaction function for the excitatory populations and **B** for the inhibitory populations. The black curve, the green curve, and the bright yellow curve represent the discrete-delay model, the Gaussian distributed delay model, and the log-normal distributed delay model, respectively. **A** shows significantly different phase-locking behavior for the Wilson-Cowan model with distributed delay. The Gaussian- and log-normal distributed delay follow qualitatively the same trajectory as the model does for discrete delay but differ in shifts of their amplitude. Fig. 6 and Fig. 7 in Appendix (B) prove that the Gaussian- and the log-normal distributed delay solution, respectively, converge to the discrete delay solution in the limit of vanishing standard deviation σ, hence

$$\lim_{\sigma \to 0} H(\phi)_{gauss} = \lim_{\sigma \to 0} H(\phi)_{log-normal} = H(\phi)_{discrete}.$$

All curves have been normalized since only the intersections with the horizontal zero line are of interest to compare the effects of different delay types.

To understand how the distribution of the delay parameters impacts phase-locked behaviors, we constructed bifurcation diagrams for the phase-locked states of excitatory-excitatory and inhibitory-inhibitory coupled pairs of identical Wilson-Cowan modules under distributed delays. While Fig. 4 displays the phase interaction functions $\mathrm{H}(\phi)$ for the delay system for one single value of the standard deviation of the delay distribution $\sigma = 0.2$, in Fig. 5 we focus on the phase-locked states of each delay type with σ-values ranging $[0, 1]$. The zeros of $\mathrm{H}(\phi)$ are phase-locked states ϕ^* of

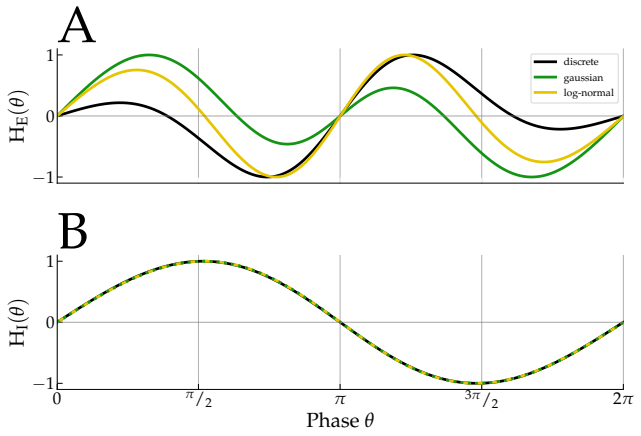

Fig. 4 Phase interaction functions for the excitatory and inhibitory populations vs phase difference ϕ. A shows the the interaction functions for the excitatory H_E and **B** for the inhibitory H_I populations. The black curve, the green curve, and the bright yellow curve represent the discrete-delay model, the Gaussian-distributed delay model, and the log-normal distributed delay model, respectively. Same parameters as in Fig. 3, except $\sigma = 0.2$ and $C = 0.01$.

the coupled system. The top panel **A** shows the phase difference of phase-locked states ϕ^*_E vs. the standard deviation σ of the Gaussian delay distribution for the excitatory populations. The middle panel **B** shows the phase difference of phase-locked states ϕ^*_E vs. the standard deviation σ of the log-normal delay distribution for the excitatory populations. The bottom panel **C** displays the same information for inhibitory-intercoupling both for the Gaussian and log-normal delay distributions. By convention, the solid lines indicate stable solutions, the dashed lines unstable solutions. The black filled circles at $\sigma = 0$ represent the stable phase-locked states for discrete delay and the black open circles mark the unstable phase-locked solutions, respectively.

We discover that for the Gaussian-delay distribution under low delay standard deviation values stable synchronous and anti-synchronous phase-locking occurs; these states are separated by an unstable partial-phase-delay state (Fig. 5**A**). Please note that diamonds show the calculated output of $\phi^*_{E\,gauss} = 0$ for $\sigma = 0.04, 0.08, ..., 0.24$, and the dashed line which connects these data points has been generated by a second order polynomial fit. We approximately find that the stable branch at $\phi^*_{E\,gauss} = \pi$ exists up to a value of $\sigma \approx 0.28$. We also note that for the whole range $\sigma = [0, 1]$ the phase-locked states for the Gaussian-delay distribution are stable for the excitatory populations at $\phi^*_{E\,gauss} = 0$ and 2π.

We observe similar behavior for the log-normal distributed delay model (Fig. 5**B**) but with a stabilizing effect on the dynamics especially at $\phi^*_{E\,log} = \pi$. With the help of the polynomial fit we approximately find on the basis of the diamonds at which $\phi^*_{E\,log} = 0$ for $\sigma = 0.04, 0.08, ..., 0.32$ that the stable branch at $\phi^*_{E\,log} = \pi$ exists up to a value of $\sigma \approx 0.35$. Additionally, we see that for the whole range $\sigma = [0, 1]$ the phase-locked states for the log-normal delay distribution are stable for the excitatory populations at $\phi^*_{E\,gauss} = 0$ and 2π.

The inhibitory populations show no difference in behavior when we compare the Gaussian and log-normal delay distribution. We obtain two stable phase-locked solutions for $\phi^*_I = 0, 2\pi$ and one unstable solution for $\phi^*_{E/I} = \pi$ for all considered delay distributions.

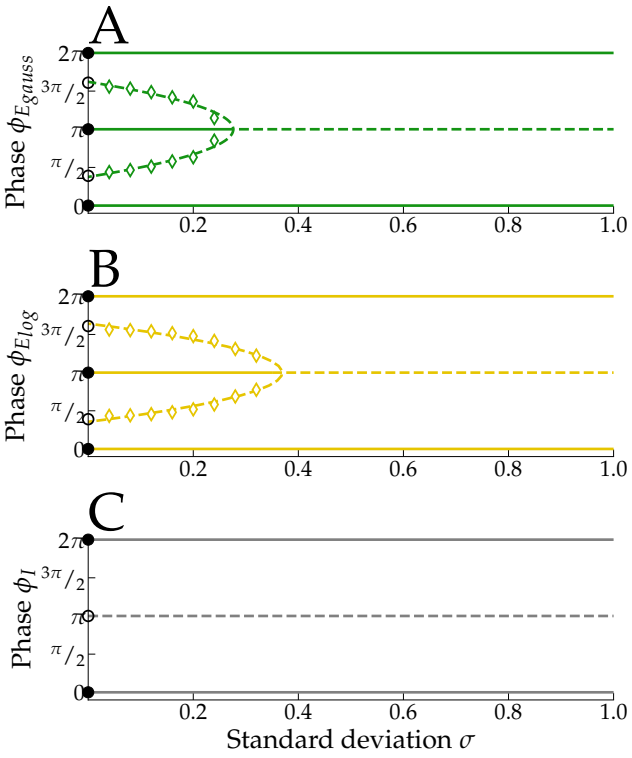

Fig. 5 Bifurcation diagram for two weakly coupled Wilson-Cowan oscillators with discrete and distributed delay. The top panel **A** shows in green the phase difference of phase-locked states $\phi^*_{E\,gauss}$ over the standard deviation σ for the excitatory cells with the Gaussian-delay distribution. The middle panel **B** shows in yellow the phase difference of phase-locked states $\phi^*_{E\,log}$ over the standard deviation σ for the excitatory cells with the log-normal-delay distribution. The bottom panel **C** displays in grey the phase difference of phase-locked states $\phi^*_{I\,gauss/log}$ over the standard deviation σ for the inhibitory cells both for the Gaussian- and log-normal-delay distribution. The solid lines indicate the stable solutions. The dashed lines the unstable solutions. The black filled dots at $\sigma = 0$ represent the stable phase-locked states for discrete delay and the black circles the unstable phase-locked solutions, respectively. The green/grey and yellow/bright-grey diamonds show the calculated output of $\phi^*_{E\,gauss/log} = 0$ for the corresponding σ-values and the dashed lines which connect these data points have been generated by a second order polynomial fit for each panel. Parameters: $\tau = -1$, $w_{ee} = 20$, $w_{ei} = 21$, $w_{ie} = 16$, $w_{ii} = 6$, $i_e = 1.5$, $i_i = -0.5$ and $C = 0.01$.

4 Discussion

Synchronization properties of inter-coupled neuronal circuits have been a focus of interest to both experimental and theoretical neuroscience for quite some time. In particular, such synchronization has been linked to both normal and pathological activity in the brain [3]: e.g. epileptic seizure [53], optimal coding under gamma oscillations [54] and directed signal transfer under the communication through coherence hypothesis [8, 32]. One of the aspects that has a significant impact on the structure of the phase-locked states of inter-coupled circuits is the delay in the synaptic coupling that can lead to synchrony, asynchrony and/or symmetry-broken states [33,55,56]. Interestingly, connection delays have been argued to play a key role in structuring brain activity, and delays that depend on spatial location of neural populations are likely to play an important role in the variety of phase locking modes seen in data [10].

Phase response curves [13–19] provide a fruitful tool to study phase coupling regimes of spiking networks and have been suggested as a causal measure of functional connectivity [33,57] and a way to assess the functional connectome of the brain [10] resulting from directed information transfer in symmetry-broken states [58].

We previously showed methodology to compute macroscopic phase response curves for emergent oscillations in large scale networks described by exact reduced mean-field equations [18]. In that work we considered discrete delays. However, discrete delays are not likely to occur in brain circuits. Recent experimental literature [31] shows non-discrete and distributed delays for non-myelinated connections in the brain. In particular, the log-normal delay distributions with large tails for long-delay values have been observed. Hence, it has been an important question of study how random distributions of delays would affect synchronization and phase locking of spiking circuits. For example, Petkoski et al. [59] showed that depending on the structure of the heterogeneity of the delays, the oscillators group in phase-shifted, anti-phase, stationary or non-stationary clusters, which introduces non-trivial spatiotemporal dynamics.

The contribution of this work is two-fold. First, we present a theoretical framework to calculate the macroscopic phase response curves of distributed-delay induced limit cycles using the adjoint method. More specifically, the mathematical formalism of the adjoint method requires a nontrivial extension of the scalar product (Eq. 9) and the normalization condition (Eq. 11) for distributed delay. We apply our technique to the Wilson-Cowan model with Gaussian and log-normal delay distributions. We find the adjoint equation and calculate the phase response curves. As a check of validity we compare the phase response curves with those obtained by the direct method and obtain good agreement.

Second, we show how the distributed delays impact phase-locking of inter-coupled circuits using oscillatory Wilson-Cowan networks as a paradigmatic example. We apply this theory to an inter-coupled pair of Wilson-Cowan oscillators and calculate the phase interaction function for each delay distribution for a given parameter set in the regime of gamma oscillations in the brain. The differences between the interaction functions for discrete, Gaussian and log-normal distributed delay in Fig. 4 indicates that the phase-locking behavior of oscillating neural systems depends on the choice of the type of delay distribution as well as its parameters.

On the one hand we observe in general that distributed delays preserve bistability between synchrony and anti-synchrony for a varying range of standard deviation σ. On the other hand, our analysis shows that synchrony becomes the only stable state beyond a critical point if the delay variance and the phase locking seen in the discrete case is conserved. In the case of the skewed log-normal distributed delay, due to the heavy tail of longer delay values, we obtain a larger bistable region than for the discrete or Gaussian-distributed case. As seen on the bifurcation diagram in Fig. 5 we show the stable and unstable phase-locked states of the three investigated types of delay. The Gaussian delay distribution shows further unstable phase-locked states for small $\sigma \lessapprox 0.28$ and the log-normal delay distribution, however, shows unstable phase-locked states for small $\sigma \lessapprox 0.35$, which vanish for increasing σ. Large tail distributions of delays like the log-normal distribution do not perturb synchrony but extend the region of bistability. Overall our analysis suggests that phase locked states can persist under highly heterogeneous delays in the brain circuits.

In conclusion, distributed delay has a significant effect upon the dynamics of networks of neural oscillators. We have shown that the symmetry properties of the delay distribution influence the dynamics, using the example of a symmetric Gaussian and an asymmetric log-normal distribution, and further that paradoxically wide delay distributions favor synchronous states.

Our study lays out a path to a number of promising research directions. For one, further research should go beyond the Wilson-Cowan model with discrete, Gaussian and log-normal delay distributions to other oscillatory systems to which our theory of phase response curves can also be applied. In this context, we could focus on the dynamics of symmetry broken states in [33] and investigate the question how such symmetry breaking maybe be modified by distributed delays. Since the nature of the delay is the focus of this work, an interesting question for the future would be how the dynamics would behave if the distribution of the delays has sufficiently heavy tails such that the mean does not exist, or distributions with non-monotonic behavior of the tails arise (e.g., if the connections between neuronal populations are clustered as a function of the distance). A next

step in a neuronal context would be to use a more detailed model focussing, e.g., on the gamma oscillation range, and to study in detail the impact of the statistical parameters of the delay distributions specifically on the structure of this gamma-activity. We suggest that our framework gives theoretical tools necessary for further studies of diverse pathological states (e.g., demyelinating diseases) which change the coupling delays and hence lead to changes in the dynamics of the brain.

Acknowledgements This work was supported by ANR-ERMUNDY.

References

1. G. Buzsáki, *Rhythms of the Brain* (Oxford University Press, 2006). URL https://oxford.universitypressscholarship.com/view/10.1093/acprof:oso/9780195301069.001.0001/acprof-9780195301069
2. G. Buzsáki, N. Logothetis, S. W., Neuron **80**(3), 751 (2013). DOI https://doi.org/10.1016/j.neuron.2013.10.002. URL http://www.sciencedirect.com/science/article/pii/S0896627313009045
3. P.J. Uhlhaas, W. Singer, Neuron **52**(1), 155 (2006). DOI doi:10.1016/j.neuron.2006.09.020. URL https://doi.org/10.1016/j.neuron.2006.09.020
4. T.H. Bullock, Proceedings of the National Academy of Sciences **94**(1), 1 (1997). DOI 10.1073/pnas.94.1.1. URL https://www.pnas.org/content/94/1/1
5. G. Buzsáki, A. Draguhn, Science **304**(5679), 1926 (2004). DOI 10.1126/science.1099745. URL https://science.sciencemag.org/content/304/5679/1926
6. G. Buzsáki, X.J. Wang, Annual Review of Neuroscience **35**(1), 203 (2012). DOI 10.1146/annurev-neuro-062111-150444. URL https://doi.org/10.1146/annurev-neuro-062111-150444. PMID: 22443509
7. M. Bartos, I. Vida, P. Jonas, Nature Reviews Neuroscience **8**(1), 45 (2007). DOI 10.1038/nrn2044. URL https://doi.org/10.1038/nrn2044
8. P. Fries, Trends in Cognitive Sciences **9**(10), 474 (2005). DOI 10.1016/j.tics.2005.08.011. URL https://doi.org/10.1016/j.tics.2005.08.011
9. M. Strüber, J.F. Sauer, P. Jonas, M. Bartos, Nature Communications **8**(1), 758 (2017). DOI 10.1038/s41467-017-00936-3. URL https://doi.org/10.1038/s41467-017-00936-3
10. P. Fries, Annual Review of Neuroscience **32**(1), 209 (2009). DOI 10.1146/annurev.neuro.051508.135603. URL https://doi.org/10.1146/annurev.neuro.051508.135603. PMID: 19400723
11. G. Deco, M.L. Kringelbach, Trends in Neurosciences **39**(3), 125 (2016). DOI 10.1016/j.tins.2016.01.001. URL https://doi.org/10.1016/j.tins.2016.01.001
12. E. Maris, P. Fries, F. van Ede, Trends in Neurosciences **39**(2), 86 (2016). DOI 10.1016/j.tins.2015.12.004. URL https://doi.org/10.1016/j.tins.2015.12.004
13. A.T. Winfree, *The Geometry of Biological Time* (Springer-Verlag New York, 2001). DOI 10.1007/978-1-4757-3484-3. URL https://doi.org/10.1007/978-1-4757-3484-3
14. E. Brown, J. Moehlis, P. Holmes, Neural Comput. **16**(4), 673 (2004). DOI 10.1162/089976604322860668. URL http://dx.doi.org/10.1162/089976604322860668
15. G.B. Ermentrout, D.H. Terman, *Mathematical Foundations of Neuroscience* (Springer New York, 2010). DOI 10.1007/978-0-387-87708-2. URL https://doi.org/10.1007/978-0-387-87708-2
16. N.W. Schultheiss, A.A. Prinz, R.J. Butera (eds.), *Phase Response Curves in Neuroscience* (Springer New York, 2012). DOI 10.1007/978-1-4614-0739-3. URL https://doi.org/10.1007/978-1-4614-0739-3
17. K. Kotani, I. Yamaguchi, Y. Ogawa, Y. Jimbo, H. Nakao, G.B. Ermentrout, Phys. Rev. Lett. **109**, 044101 (2012). DOI 10.1103/PhysRevLett.109.044101. URL https://link.aps.org/doi/10.1103/PhysRevLett.109.044101
18. G. Dumont, G.B. Ermentrout, B. Gutkin, Phys. Rev. E **96**, 042311 (2017). DOI 10.1103/PhysRevE.96.042311. URL https://link.aps.org/doi/10.1103/PhysRevE.96.042311
19. B. Monga, D. Wilson, T. Matchen, J. Moehlis, Biological Cybernetics **113**(1-2), 11 (2018). DOI 10.1007/s00422-018-0780-z. URL https://doi.org/10.1007/s00422-018-0780-z
20. C.C. Canavier, S. Achuthan, Mathematical Biosciences **226**(2), 77 (2010). DOI https://doi.org/10.1016/j.mbs.2010.05.001. URL https://www.sciencedirect.com/science/article/pii/S0025556410000714
21. F.C. Hoppensteadt, E.M. Izhikevich, *Weakly Connected Neural Networks* (Springer New York, 1997). DOI 10.1007/978-1-4612-1828-9. URL https://doi.org/10.1007/978-1-4612-1828-9
22. D. Kuelbs, J. Dunefsky, B. Monga, J. Moehlis, Biological Cybernetics **114**(6), 589 (2020). DOI 10.1007/s00422-020-00850-w. URL https://doi.org/10.1007/s00422-020-00850-w
23. B. Ermentrout, Neural Computation **8**(5), 979 (1996). DOI 10.1162/neco.1996.8.5.979. URL https://doi.org/10.1162/neco.1996.8.5.979
24. M.A. Schwemmer, T.J. Lewis, *The Theory of Weakly Coupled Oscillators* (Springer New York, New York, NY, 2012), pp. 3–31. DOI 10.1007/978-1-4614-0739-3_1. URL https://doi.org/10.1007/978-1-4614-0739-3_1
25. J. Bueno, D. Brunner, M.C. Soriano, I. Fischer, Opt. Express **25**(3), 2401 (2017). DOI 10.1364/oe.25.002401. URL https://doi.org/10.1364/OE.25.002401
26. G. Giacomelli, M. Calzavara, F. Arecchi, Optics Communications **74**(1), 97 (1989). DOI https://doi.org/10.1016/0030-4018(89)90498-7. URL https://www.sciencedirect.com/science/article/pii/0030401889904987
27. K.E. Callan, L. Illing, Z. Gao, D.J. Gauthier, E. Schöll, Phys. Rev. Lett. **104**, 113901 (2010). DOI 10.1103/PhysRevLett.104.113901. URL https://link.aps.org/doi/10.1103/PhysRevLett.104.113901
28. M.C. Soriano, J. García-Ojalvo, C.R. Mirasso, I. Fischer, Rev. Mod. Phys. **85**, 421 (2013). DOI 10.1103/RevModPhys.85.421. URL https://link.aps.org/doi/10.1103/RevModPhys.85.421
29. K.E. Callan, L. Illing, Z. Gao, D.J. Gauthier, E. Schöll, Phys. Rev. Lett. **104**, 113901 (2010). DOI 10.1103/PhysRevLett.104.113901. URL https://link.aps.org/doi/10.1103/PhysRevLett.104.113901
30. D.P. Rosin, K.E. Callan, D.J. Gauthier, E. Schöll, EPL (Europhysics Letters) **96**(3), 34001 (2011). DOI 10.1209/0295-5075/96/34001. URL https://doi.org/10.1209/0295-5075/96/34001
31. G. Buzsáki, K. Mizuseki, Nature Reviews Neuroscience **15**(4), 264 (2014). DOI 10.1038/nrn3687. URL https://doi.org/10.1038/nrn3687
32. T. Womelsdorf, J.M. Schoffelen, R. Oostenveld, W. Singer, R. Desimone, A.K. Engel, P. Fries, Science **316**(5831), 1609 (2007). DOI 10.1126/science.1139597. URL https://doi.org/10.1126/science.1139597
33. G. Dumont, B. Gutkin, PLOS Computational Biology **15**(5), 1 (2019). DOI 10.1371/journal.pcbi.1007019. URL https://doi.org/10.1371/journal.pcbi.1007019

34. H.R. Wilson, J.D. Cowan, Biophysical Journal **12**(1), 1 (1972). DOI 10.1016/s0006-3495(72)86068-5. URL https://doi.org/10.1016/s0006-3495(72)86068-5
35. F.C. Hoppensteadt, E.M. Izhikevich, *Weakly Connected Neural Networks* (Springer New York, 1997). DOI 10.1007/978-1-4612-1828-9. URL https://doi.org/10.1007/978-1-4612-1828-9
36. W. Just, A. Pelster, M. Schanz, E. Schöll, Philosophical Transactions of the Royal Society A: Mathematical, Physical and Engineering Sciences **368**(1911), 303 (2010). DOI 10.1098/rsta.2009.0243. URL https://doi.org/10.1098/rsta.2009.0243
37. K. Lüdge, B. Lingnau, *Laser Dynamics and Delayed Feedback* (Springer US, New York, NY, 2020), pp. 31–47. DOI 10.1007/978-1-0716-0421-2_729. URL https://doi.org/10.1007/978-1-0716-0421-2_729
38. J.F. Totz, J. Rode, M.R. Tinsley, K. Showalter, H. Engel, Nature Physics **14**(3), 282 (2017). DOI 10.1038/s41567-017-0005-8. URL https://doi.org/10.1038/s41567-017-0005-8
39. J.G. Milton, IFAC-PapersOnLine **48**(12), 87 (2015). DOI 10.1016/j.ifacol.2015.09.358. URL https://doi.org/10.1016/j.ifacol.2015.09.358. 12th IFAC Workshop onTime Delay SystemsTDS 2015
40. L. Glass, Nature **410**(6825), 277 (2001). DOI 10.1038/35065745. URL https://doi.org/10.1038/35065745
41. S.G. WAXMAN, M.V.L. BENNETT, Nature New Biology **238**(85), 217 (1972). DOI 10.1038/newbio238217a0. URL https://doi.org/10.1038/newbio238217a0
42. G. Aumüller, G. Aust, A. Conrad, J. Engele, J. Kirsch, G. Maio, A. Mayerhofer, S. Mense, D. Reißig, J. Salvetter, W. Schmidt, F. Schmitz, E. Schulte, K. Spanel-Borowski, G. Wennemuth, W. Wolff, L.J. Wurzinger, H.G. Zilch, *Duale Reihe Anatomie* (Georg Thieme Verlag, 2020). DOI 10.1055/b-007-170976. URL https://doi.org/10.1055/b-007-170976
43. K. Pyragas, Physics Letters A **170**(6), 421 (1992). DOI 10.1016/0375-9601(92)90745-8. URL https://doi.org/10.1016/0375-9601(92)90745-8
44. Y.N. Kyrychko, K.B. Blyuss, E. Schöll, Chaos: An Interdisciplinary Journal of Nonlinear Science **24**(4), 043117 (2014). DOI 10.1063/1.4898771. URL https://doi.org/10.1063/1.4898771
45. F.M. Atay, Physical Review Letters **91**(9) (2003). DOI 10.1103/physrevlett.91.094101. URL https://doi.org/10.1103/physrevlett.91.094101
46. C. Wille, J. Lehnert, E. Schöll, Physical Review E **90**(3) (2014). DOI 10.1103/physreve.90.032908. URL https://doi.org/10.1103/physreve.90.032908
47. Y.N. Kyrychko, K.B. Blyuss, E. Schöll, The European Physical Journal B **84**(2), 307 (2011). DOI 10.1140/epjb/e2011-20677-8. URL https://doi.org/10.1140/epjb/e2011-20677-8
48. Y.N. Kyrychko, K.B. Blyuss, E. Schöll, Philosophical Transactions of the Royal Society A: Mathematical, Physical and Engineering Sciences **371**(1999), 20120466 (2013). DOI 10.1098/rsta.2012.0466. URL https://doi.org/10.1098/rsta.2012.0466
49. F.M. Atay, A. Hutt, SIAM Journal on Applied Dynamical Systems **5**(4), 670 (2006). DOI 10.1137/050629367. URL https://doi.org/10.1137/050629367
50. X. Liang, M. Tang, M. Dhamala, Z. Liu, Physical Review E **80**(6) (2009). DOI 10.1103/physreve.80.066202. URL https://doi.org/10.1103/physreve.80.066202
51. U. Meyer, J. Shao, S. Chakrabarty, S.F. Brandt, H. Luksch, R. Wessel, Biological Cybernetics **99**(1), 79 (2008). DOI 10.1007/s00422-008-0239-8. URL https://doi.org/10.1007/s00422-008-0239-8
52. I. Omelchenko, O.E. Omel'chenko, P. Hövel, E. Schöll, Physical Review Letters **110**(22) (2013). DOI 10.1103/physrevlett.110.224101. URL https://doi.org/10.1103/physrevlett.110.224101
53. G. Deco, V. Jirsa, A.R. McIntosh, O. Sporns, R. Kotter, Proceedings of the National Academy of Sciences **106**(25), 10302 (2009). DOI 10.1073/pnas.0901831106. URL https://doi.org/10.1073/pnas.0901831106
54. M. Chalk, B. Gutkin, S. Denève, eLife **5** (2016). DOI 10.7554/elife.13824. URL https://doi.org/10.7554/elife.13824
55. D. Reyner-Parra, G. Huguet, bioRxiv (2021). DOI 10.1101/2021.08.13.456218. URL https://www.biorxiv.org/content/early/2021/08/13/2021.08.13.456218
56. S. Petkoski, V.K. Jirsa, Philosophical Transactions of the Royal Society A: Mathematical, Physical and Engineering Sciences **377**(2153), 20180132 (2019). DOI 10.1098/rsta.2018.0132. URL https://doi.org/10.1098/rsta.2018.0132
57. A. Pariz, I. Fischer, A. Valizadeh, C. Mirasso, PLOS Computational Biology **17**(4), 1 (2021). DOI 10.1371/journal.pcbi.1008129. URL https://doi.org/10.1371/journal.pcbi.1008129
58. D. Battaglia, A. Witt, F. Wolf, T. Geisel, PLOS Computational Biology **8**(3), 1 (2012). DOI 10.1371/journal.pcbi.1002438. URL https://doi.org/10.1371/journal.pcbi.1002438
59. S. Petkoski, A. Spiegler, T. Proix, P. Aram, J.J. Temprado, V.K. Jirsa, Phys. Rev. E **94**, 012209 (2016). DOI 10.1103/PhysRevE.94.012209. URL https://link.aps.org/doi/10.1103/PhysRevE.94.012209

Appendix A

Derivation of the Adjoint Equation

To derive the adjoint equation for dynamics with distributed delay with the phase response curve $\mathrm{Z}(t)$ and the perturbed linearized variable $\mathrm{X_p}(t)$, we must show that:

$$\langle \mathrm{Z}(t), \mathrm{X_p}(t) \rangle \stackrel{!}{=} \text{ const.}$$

where $\mathrm{Z}(t) \in \mathbb{R}^N$ and $\mathrm{X_p}(t) \in \mathbb{R}^N$ are row vectors of N real components.
We prove this by showing that:

$$\frac{\mathrm{d}}{\mathrm{dt}} \langle \mathrm{Z}(t), \mathrm{X_p}(t) \rangle \stackrel{!}{=} 0 \tag{14}$$

with the scalar product defined as

$$\langle \Psi(t), \Phi(t) \rangle = \Psi(t)\Phi(t) + \int_0^{+\infty} ds\ \Delta(s) \int_{t-s}^{t} d\xi\ \ \Psi(\xi+s)\, \mathrm{DF_2}(\xi+s)\, \Phi(\xi) \tag{15}$$

where $\mathrm{DF_2}(t)$ is the Jacobian with respect to the delayed term of the perturbed linearized equation $\frac{\mathrm{d}}{\mathrm{dt}}\mathrm{X_p}(t) = \mathrm{DF_1}(t)\mathrm{X_p}(t) + \mathrm{DF_2}(t) \int_0^{+\infty} ds\ \Delta(s)\mathrm{X_p}(t-s)$. We apply the scalar product to Eq. (14) and obtain:

$$\Leftrightarrow \frac{\mathrm{d}}{\mathrm{dt}} \left[\mathrm{Z}(t)\mathrm{X_p}(t) + \int_0^{+\infty} ds\ \Delta(s) \int_{t-s}^{t} d\xi\ \ \mathrm{Z}(\xi+s)\, \mathrm{F_2}(\xi+s)\, \mathrm{P}(\xi) \right] = 0$$

We obtain:

$$\begin{aligned} \Leftrightarrow & \left(\frac{\mathrm{d}}{\mathrm{dt}} \mathrm{Z}(t) \right) \mathrm{X_p}(t) \\ & + \mathrm{Z}(t) \frac{\mathrm{d}}{\mathrm{dt}} \mathrm{X_p}(t) \\ & + \frac{\mathrm{d}}{\mathrm{dt}} \int_0^{+\infty} ds\ \Delta(s) \int_{t-s}^{t} d\xi\ \ \mathrm{Z}(\xi+s)\, \mathrm{DF_2}(\xi+s)\, \mathrm{X_p}(\xi) = 0 \end{aligned}$$

Taking the derivatives of the intgrals:

$$\begin{aligned} \Leftrightarrow & \left(\frac{\mathrm{d}}{\mathrm{dt}} \mathrm{Z}(t) \right) \mathrm{X_p}(t) \\ & + \mathrm{Z}(t) \frac{\mathrm{d}}{\mathrm{dt}} \mathrm{X_p}(t) \\ & + \int_0^{+\infty} ds\ \Delta(s)\, \mathrm{Z}(t+s)\, \mathrm{DF_2}(t+s)\, \mathrm{X_p}(t) \\ & - \int_0^{+\infty} ds\ \Delta(s)\, \mathrm{Z}(t)\, \mathrm{DF_2}(t)\, \mathrm{X_p}(t-s) = 0 \end{aligned}$$

We apply $\frac{\mathrm{d}}{\mathrm{dt}}\mathrm{X_p}(t) = \mathrm{DF_1}(t)\mathrm{X_p}(t) + \mathrm{DF_2}(t) \int_0^{+\infty} ds\ \Delta(s)\mathrm{X_p}(t-s)$ and simplify the integral:

$$\begin{aligned} \Leftrightarrow & \left(\frac{\mathrm{d}}{\mathrm{dt}} \mathrm{Z}(t) \right) \mathrm{X_p}(t) \\ & + \mathrm{Z}(t) \left[\mathrm{DF_1}(t)\mathrm{X_p}(t) + \mathrm{DF_2}(t) \int_0^{+\infty} ds\ \Delta(s)\mathrm{P}(t-s) \right] \\ & + \int_0^{+\infty} ds\ \Delta(s)\, \mathrm{Z}(t+s)\, \mathrm{DF_2}(t+s)\, \mathrm{X_p}(t) \\ & - \mathrm{Z}(t)\, \mathrm{DF_2}(t) \int_0^{+\infty} ds\ \Delta(s)\, \mathrm{X_p}(t-s) = 0 \end{aligned}$$

We factorize the bracket and obtain:

$$\begin{aligned} \Leftrightarrow & \left(\frac{\mathrm{d}}{\mathrm{dt}} \mathrm{Z}(t) \right) \mathrm{X_p}(t) \\ & + \mathrm{Z}(t)\mathrm{F_1}(t)\mathrm{X_p}(t) \\ & + \mathrm{Z}(t)\mathrm{F_2}(t) \int_0^{+\infty} ds\ \Delta(s)\mathrm{P}(t-s) \\ & + \int_0^{+\infty} ds\ \Delta(s)\, \mathrm{Z}(t+s)\, \mathrm{F_2}(t+s)\, \mathrm{X_p}(t) \\ & - \mathrm{Z}(t)\, \mathrm{F_2}(t) \int_0^{+\infty} ds\ \Delta(s)\, \mathrm{P}(t-s) = 0 \end{aligned}$$

The 3rd and the 5th term cancel, and we obtain:

$$\Leftrightarrow \Bigg[\underbrace{\frac{\mathrm{d}}{\mathrm{dt}} \mathrm{Z}(t) + \mathrm{Z}(t)\mathrm{DF_1}(t) + \int_0^{+\infty} ds\ \Delta(s)\, \mathrm{Z}(t+s)\, \mathrm{DF_2}(t+s)}_{\stackrel{!}{=}0} \Bigg] \mathrm{X_p}(t) = 0 \tag{16}$$

Since this condition holds for arbitrary solutions $\mathrm{X_p}(t)$, the bracket vanishes and we obtain the adjoint equation for distributed delay dynamics:

$$\Rightarrow -\frac{\mathrm{d}}{\mathrm{dt}} \mathrm{Z}(t) = \mathrm{DF_1^T}(t)\mathrm{Z}(t) + \int_0^{+\infty} ds\ \Delta(s)\, \mathrm{DF_2^T}(t+s)\, \mathrm{Z}(t+s) \tag{17}$$

where superscript T denotes the transposed matrix.

□

Appendix B

Gaussian Distributed Delay Convergence

Fig. 6 represents in the panels **A** and **B** phase response curves for excitatory $\mathrm{Z_E}(\phi)$ and inhibitory $\mathrm{Z_I}(\phi)$ populations, respectively. Panels **C** and **D** display the interaction functions for excitatory $\mathrm{H_E}(\phi)$ and inhibitory $\mathrm{H_I}(\phi)$ populations. The black solid curve in each subplot shows the discrete delay solution and from bright to dark color the solutions for the Gaussian distributed model for decreasing standard deviation values σ. This figure reveals that the Gaussian delay distribution is approaching the discrete delay solution for vanishing values of the standard deviation σ.

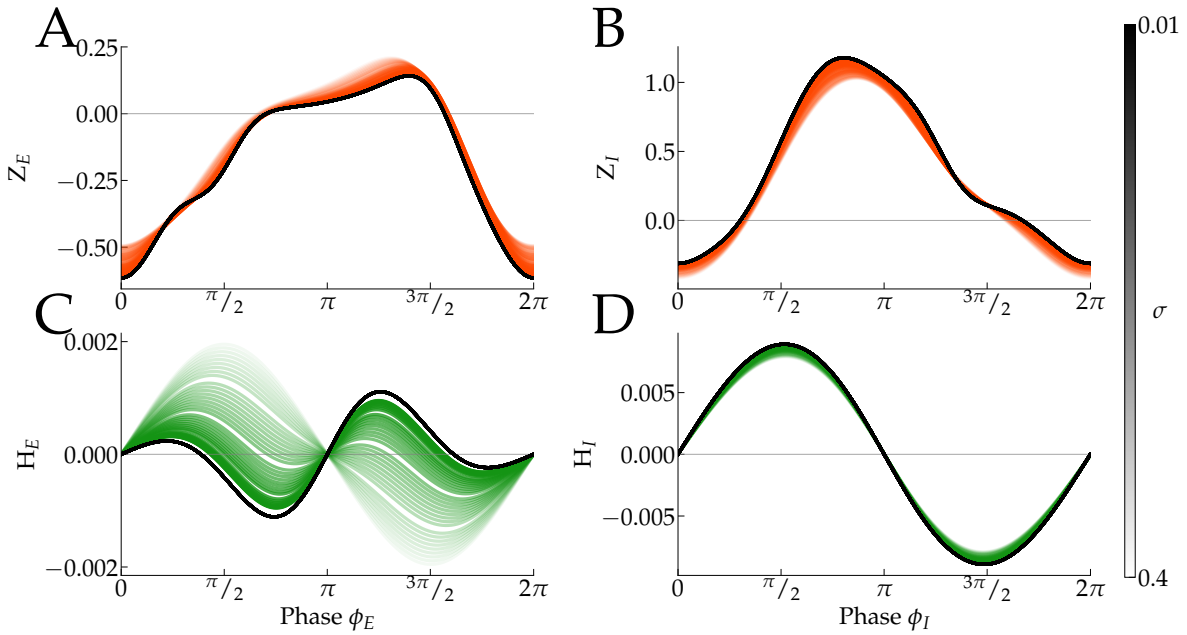

Fig. 6 Wilson-Cowan oscillators with Gaussian distributed delay converge to discrete delay model. The panels **A** and **B** show the phase response curves for excitatory $Z_E(\phi)$ and inhibitory $Z_I(\phi)$ populations, respectively. Panels **C** and **D** display the interaction functions for excitatory $H_E(\phi)$ and inhibitory $H_I(\phi)$ populations. Each subplot shows as the black solid curve the discrete delay solution and from bright to dark color solutions for the Gaussian distributed model for decreasing standard deviation values σ. Parameters: $\sigma = 0.01, 0.02, 0.03, ..., 0.4$ from dark to light shading , $\tau = -1$, $w_{ee} = 20$, $w_{ei} = 21$, $w_{ie} = 16$, $w_{ii} = 6$, $i_e = 1.5$, $i_i = -0.5$ and $C = 0.01$.

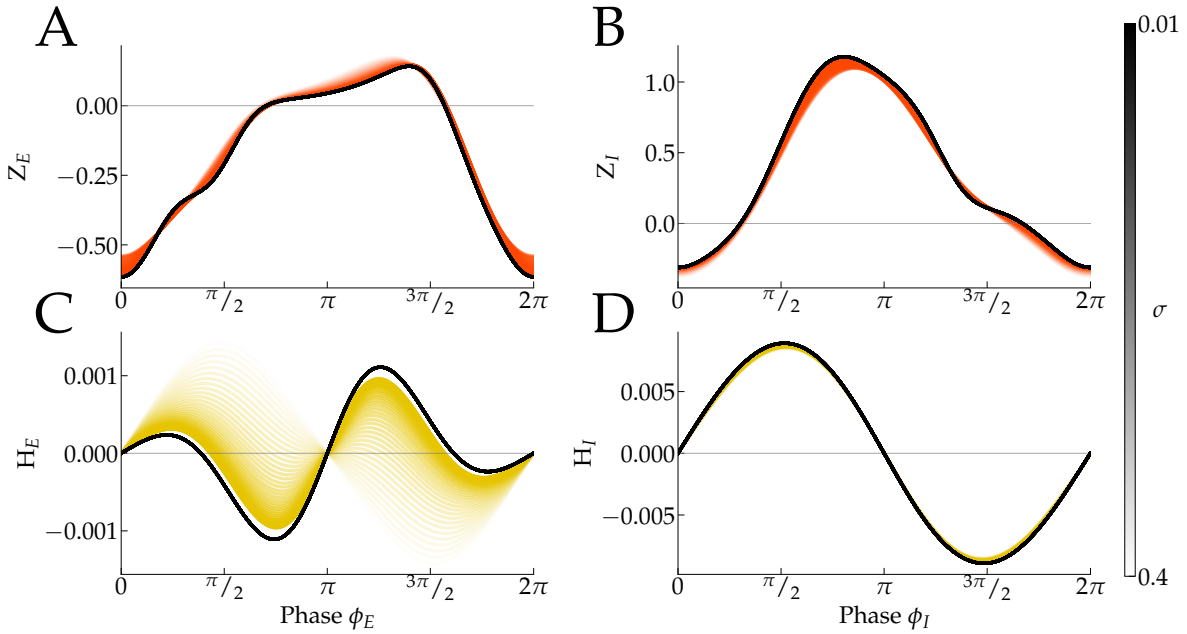

Fig. 7 Wilson-Cowan oscillators with log-normal distributed delay converge to discrete delay model. The panels **A** and **B** show the phase response curves for excitatory $Z_E(\phi)$ and inhibitory $Z_I(\phi)$ populations, respectively. Panels **C** and **D** display the interaction functions for excitatory $H_E(\phi)$ and inhibitory $H_I(\phi)$ populations. Each subplot shows as the black solid curve the discrete delay solution and from bright to dark color solutions for the log-normal distributed model for decreasing standard deviation values σ. Parameters: $\sigma = 0.01, 0.02, 0.03, ..., 0.4$ from dark to light shading , $\tau = -1$, $w_{ee} = 20$, $w_{ei} = 21$, $w_{ie} = 16$, $w_{ii} = 6$, $i_e = 1.5$, $i_i = -0.5$ and $C = 0.01$.